Dynamical N-body simulations of Coulomb scattering in plasma sheaths

R. T. Farouki, S. Hamaguchi, M. Surendra, and M. Dalvie
IBM Thomas J. Watson Research Center, P.O. Box 218, Yorktown Heights, New York 10598
(Received 7 May 1992)

N-body simulations are used to assess the importance of discrete ion-ion Coulomb interactions in an electron-free plasma sheath, where ordinary Debye screening is ineffective. The angular dispersion $\theta_{\rm rms}$ of the ion flux incident on the cathode is found to have a power-law dependence on a parameter Ω measuring the "graininess" of the sheath electric field, and an explanation for the observed exponent in this relation is postulated in terms of diffusion theory. In the *Coulomb logarithm,* a lower cutoff $b_{\rm min}$ equal to a fraction of the mean ion-ion distance at the plasma-sheath boundary is determined, while the upper cutoff $b_{\rm max}$ appears to be no more than about ten times the sheath thickness d; no sustained logarithmic growth of $\theta^2_{\rm rms}$ with the lateral extent a over which Coulomb interactions are taken into account was observed. For sheath parameters representative of the low-pressure weakly ionized discharges used in very-large-scale-integration manufacturing processes, the dispersion due to Coulomb scattering in the sheath is typically $\theta_{\rm rms} \lesssim 0.1°$.

PACS number(s): 52.20.−j, 52.40.Hf, 52.65.+z

I. INTRODUCTION

For a quasineutral plasma, it is customary to ignore long-range Coulomb interactions between charged particles over length scales exceeding the Debye length λ_D when assessing the perturbative effect of such interactions upon the trajectory of an individual "test particle." This remedies a logarithmic divergence of the *dynamical-friction* and *velocity-diffusion* coefficients, which measure the rate at which the test particle's systematic velocity decays and the growth of its random longitudinal and transverse velocity components [1], and is physically plausible on the grounds that the highly mobile electron gas redistributes over length scales $\gtrsim \lambda_D$ so as to effectively "screen" externally imposed fields or Coulomb forces between particles.

However, in a plasma *sheath,* i.e., the extended region of positive space charge and depleted electron density that forms adjacent to any material surface in contact with the plasma, ordinary Debye screening is inoperative, and the degree to which discrete Coulomb interactions can influence the trajectories of ions as they flow across the sheath is uncertain. (The lateral extent of the sheath, determined by the surface dimensions, is typically much larger than its thickness, which in turn is usually many Debye lengths.)

A similar dilemma arises in another physical context where unscreened Coulomb forces act over large distances: the gravitational N-body problem. In self-gravitating systems such as star clusters and galaxies, Chandrasekhar [2] has argued that two-body encounters at distances appreciably greater than the mean interparticle spacing l may be neglected (see also [3]), whereas empirical estimates of the *Coulomb logarithm* —based on monitoring the secular evolution of bound clusters in numerical simulations [4]—suggest, on the contrary, that interactions on all length scales up to the characteristic system dimension L contribute to "relaxation" effects.

Apart from its theoretical interest, the problem of assessing the role of discrete Coulomb forces in sheaths may also be of practical importance in the plasma processing of semiconductor materials [5]. Current very-large-scale-integration (VLSI) designs call for reactive-ion etching of deep "trenches" with very high aspect ratios, for which an angular dispersion of 1° or less from a strictly collimated ion flux across the sheath might have discernible manufacturing implications.

While there has been considerable effort recently in modeling the angular and energy distribution of ions accelerated across the sheaths of low-pressure dc and rf discharges [6–10], these studies have universally ignored the two-body Coulomb interactions of ions. This is often justified by the observation that, under typical process-plasma conditions, the ionization fraction f_i of the discharge gas is very low—typically 10^{-3} or less.

It should be noted, however, that the mean ion-ion distance exceeds the mean ion-neutral distance only by a factor $\sim f_i^{-1/3}$. Since Coulomb forces have a much greater "reach" than those between ions and neutrals—e.g., polarization attraction [11]—the argument cited above is not convincing. (Of course, if the sheath thickness d is *not* much smaller than the mean free path $\lambda_{\rm mfp}$ for "direct collisions" with neutrals, in which short-range forces induce large deflections, the angular distribution of the incident-ion flux will be totally dominated by ion-neutral scattering.)

In this paper we report on numerical experiments designed to reexamine the unscreened Coulomb force problem, within the plasma-sheath context, from first principles. We appeal to a direct N-body scheme, in which particle motions are integrated under forces obtained by an explicit summation over pairwise interactions (see Appendix A). This approach is computationally very expensive, but it faithfully reproduces the stochastic nature of the forcefield experienced by each particle, and allows for very accurate integration of small-angle deflections—unlike traditional particle-mesh schemes [12] used to simulate macroscopic plasma phenomena.

However, since the particle number N cannot exceed $\sim 10^4$ in practice, the behavior of physical systems can only be inferred by bold extrapolation of the simulation results.

II. SUMMARY OF RELATED THEORY

Before proceeding to the N-body simulations, we first give a brief synopsis of existing theory for particle transport in a stochastic Coulomb field, and assess its suitability to the plasma sheath context. The change in velocity of a "test" particle moving under the Coulomb influence of a background of "field" particles has been studied in detail by Chandrasekhar, in the context of stellar dynamics [2] (see also [13,14]). In the case of plasma systems, Spitzer [1] summarizes Chandrasekhar's results as follows: For a test particle of mass m and charge q moving at speed v relative to a background of similar field particles having uniform number density n and a Maxwellian velocity distribution characterized by temperature T, the change of v is described approximately by the quantities

$$\langle \Delta v_{\parallel} \rangle = -\frac{q^4 n \ln\Lambda}{2\pi\epsilon_0^2 m k T}\left[\frac{\mathrm{erf}(x)}{2x^2} - \frac{\exp(-x^2)}{\sqrt{\pi}x}\right] \tag{1}$$

and

$$\langle (\Delta v_{\parallel})^2 \rangle = \frac{q^4 n \ln\Lambda}{2\pi\epsilon_0^2 m^2 v}\left[\frac{\mathrm{erf}(x)}{2x^2} - \frac{\exp(-x^2)}{\sqrt{\pi}x}\right],$$
$$\langle (\Delta v_{\perp})^2 \rangle = \frac{q^4 n \ln\Lambda}{2\pi\epsilon_0^2 m^2 v}\left[\mathrm{erf}(x) - \frac{\mathrm{erf}(x)}{2x^2} + \frac{\exp(-x^2)}{\sqrt{\pi}x}\right], \tag{2}$$

where $x=(mv^2/2kT)^{1/2}$ and $\mathrm{erf}(x)$ denotes the "error function"

$$\mathrm{erf}(x) = \frac{2}{\sqrt{\pi}}\int_0^x \exp(-t^2)dt\ . \tag{3}$$

Here, $\ln\Lambda$ is the "Coulomb logarithm," $\Lambda = b_{\max}/b_{\min}$ being the ratio of the largest to the smallest impact parameters of Coulomb interactions that have been taken into consideration. Clearly, we require $b_{\min} > 0$ and $b_{\max} < \infty$ for the quantities (1) and (2) to have finite values.

The quantity $\langle \Delta v_{\parallel} \rangle$ is the "dynamical-friction" coefficient—it measures the rate at which the test particle is *systematically* slowed down (dynamical friction always opposes the particle's sense of motion, as indicated by the minus sign). The longitudinal and transverse velocity "diffusion" coefficients $\langle (\Delta v_{\parallel})^2 \rangle$ and $\langle (\Delta v_{\perp})^2 \rangle$ give the rate of increase of the mean square *random* velocity components, parallel and perpendicular to the sense of motion. [Expressions (1) and (2) represent only the "dominant" dynamical-friction and diffusion terms—namely, those that are proportional to $\ln\Lambda$; in special circumstances, other terms may be of comparable or even greater magnitude.]

If Eqs. (1) and (2) are used to describe the effect of ion-ion collisions in a weakly coupled quasineutral plasma, it is customary to take

$$b_{\max} = \left[\frac{\epsilon_0 kT}{e^2 n}\right]^{1/2} \quad \text{and} \quad b_{\min} = \frac{e^2}{4\pi\epsilon_0 kT} \tag{4}$$

in the ratio $\Lambda = b_{\max}/b_{\min}$ (assuming unit-charge ions and full ionization). Here, $b_{\max}$ is the Debye length, while $b_{\min}$ is the Landau length—the closest approach of two ions moving at the characteristic thermal speed. Due to the absence of thermal equilibrium and Debye screening, however, these values are not applicable in the sheath context (values of $b_{\max}$ and $b_{\min}$ appropriate to plasma sheaths will be discussed in Sec. V below).

Now the relevance of expressions (1) and (2) to the problem of assessing how much angular dispersion discrete Coulomb interactions induce in the ion flux traversing a sheath seems tenuous at best. The nominal sheath structure involves strong density gradients and rapid streaming motions (see Sec. III below); any random motions about the stream velocity are likely non-Maxwellian and anisotropic. Furthermore, these random motions arise (in part, at least) from the Coulomb interactions themselves—any "temperature" we associate with them cannot be regarded as a fixed, *ad hoc* parameter. Since every ion must serve as both a "test" and a "field" particle, the approximation of an invariant background distribution is invalid.

The Fokker-Planck equation [15] offers a more sophisticated approach, where the coefficients (1) and (2) are generalized to non-Maxwellian systems and are then used to formulate an equation satisfied by the steady-state distribution function (see, for example [16–18]). In the present context, however, this yields a nonlinear, partial integro-differential equation that is not easy to treat analytically. We shall see in Sec. VI below that, using just the elementary theory described above, we can formulate plausible explanations for certain scaling relationships observed in the simulations.

III. NOMINAL (CONTINUUM) SHEATH MODEL

We consider a collisionless sheath, i.e., one in which the mean free path λ_{mfp} for collisions of ions with neutrals greatly exceeds the sheath thickness d, and we assume that ionization within the sheath is negligible. We also ignore electrons, assuming that their density drops rapidly within the sheath. The sheath structure is then governed only by the space-charge-limited motion of ions from the plasma-sheath boundary ($z=0$) to the cathode ($z=d$).

Let $F=n_0 u_0$ be the flux of ions, of charge q and mass m, incident on the plane $z=0$ from the plasma. Here, n_0 is the number density of ions and electrons (assumed equal) at the plasma-sheath boundary, and the directed initial velocity u_0 of ions is assumed to satisfy the Bohm criterion [19]:

$$u_0 \geq \left[\frac{kT_e}{m}\right]^{1/2}, \tag{5}$$

where T_e is the electron temperature for the plasma bulk (see also [20]).

If discrete Coulomb interactions between ions are

neglected, the sheath profiles for the ion number density $n(z)$ and stream velocity $u(z)$, and the electrostatic potential $V(z)$, are governed by a modified form [21] of the "Child-Langmuir law." By conservation of energy and ion flux, we have

$$u(z)=[u_0^2-2qV(z)/m]^{1/2} \quad \text{and} \quad n(z)u(z)=n_0u_0 , \tag{6}$$

and on substituting the above into Poisson's equation

$$d^2V/dz^2=-qn(z)/\epsilon_0 ,$$

we obtain the second-order, nonlinear equation

$$\frac{d^2V}{dz^2}=-\frac{qn_0u_0}{\epsilon_0(u_0^2-2qV/m)^{1/2}} \tag{7}$$

for the potential, which is to be solved subject to the initial conditions

$$V(0)=0 \quad \text{and} \quad \left.\frac{dV}{dz}\right|_{z=0}=-E_0 , \tag{8}$$

E_0 being the electric field at the plasma-sheath boundary.

It is convenient to introduce dimensionless variables for time, distance, and the ion density and stream velocity as follows:

$$\tau=\omega_p t, \quad \zeta=\frac{z}{\lambda_D}, \quad \nu=\frac{n}{n_0}, \quad \eta=\frac{u}{u_0} , \tag{9}$$

where

$$\omega_p=(q^2n_0/\epsilon_0m)^{1/2} \quad \text{and} \quad \lambda_D=(\epsilon_0mu_0^2/q^2n_0)^{1/2} \tag{10}$$

represent the (ion) plasma frequency and the Debye length—if we take $u_0^2=kT_e/m$—at the plasma-sheath boundary. Similarly, we adopt

$$\Phi=\frac{qV}{mu_0^2} \quad \text{and} \quad \mathcal{E}=-\frac{d\Phi}{d\zeta}=\frac{q\lambda_DE}{mu_0^2} \tag{11}$$

as the dimensionless forms of the potential $V(z)$ and electric field $E(z)$. The initial-value problem defined by (7) and (8) then becomes

$$\frac{d^2\Phi}{d\zeta^2}=-\frac{1}{\sqrt{1-2\Phi}} \quad \text{with } \Phi(0)=0, \quad \left.\frac{d\Phi}{d\zeta}\right|_{\zeta=0}=-\mathcal{E}_0 \tag{12}$$

(where $\mathcal{E}_0=q\lambda_DE_0/mu_0^2$). The general solution to (12) is somewhat involved; we summarize it below and refer the reader to [21] for further details.

Obviously, $\Phi(\zeta)$ depends only on the single parameter $\mathcal{E}_0$. In general, it satisfies a cubic equation of the form

$$(1-2\Phi)^3+c_2(1-2\Phi)^2+c_1(1-2\Phi)+c_0=0 , \tag{13}$$

where, in terms of the quantities

$$Q(\zeta)=\frac{9\zeta^2}{2}+3\mathcal{E}_0(3-\mathcal{E}_0^2)\zeta+4-\frac{3\mathcal{E}_0^2}{2} \quad \text{and} \quad K=\frac{\mathcal{E}_0^2}{2}-1 , \tag{14}$$

the coefficients c_2,c_1,c_0 may be expressed as

$$c_2=-9K^2, \quad c_1=-6KQ(\zeta), \quad c_0=-Q^2(\zeta) . \tag{15}$$

It may be shown [21] that if the quantity K is sufficiently small, namely, that if the condition

$$\mathcal{E}_0<(\tfrac{8}{3})^{1/2} \tag{16}$$

is satisfied, then Eq. (13) has a unique real root for all $\zeta\geq 0$. The solution to Eq. (13) may then be given in closed form as

$$1-2\Phi(\zeta)=3K^2+[\sqrt{A(\zeta)}+B(\zeta)]^{1/3}-[\sqrt{A(\zeta)}-B(\zeta)]^{1/3} , \tag{17}$$

where the polynomials $A(\zeta)$ and $B(\zeta)$ are given in terms of (14) by

$$A(\zeta)=Q^3(\zeta)[\tfrac{1}{4}Q(\zeta)+K^3] ,$$
$$B(\zeta)=\tfrac{1}{2}Q^2(\zeta)+9K^3Q(\zeta)+27K^6 . \tag{18}$$

Using Eqs. (6), the dimensionless ion stream velocity and number density may be expressed in terms of (17) as

$$\eta(\zeta)=\sqrt{1-2\Phi(\zeta)}=1/\nu(\zeta) .$$

Equivalently [21], we have

$$\eta(\zeta)=K+[\sqrt{C(\zeta)}+D(\zeta)]^{1/3}-[\sqrt{C(\zeta)}-D(\zeta)]^{1/3}=\frac{1}{\nu(\zeta)} , \tag{19}$$

where $C(\zeta)$ and $D(\zeta)$ are the polynomials

$$C(\zeta)=Q(\zeta)[\tfrac{1}{4}Q(\zeta)+K^3], \quad D(\zeta)=\tfrac{1}{2}Q(\zeta)+K^3 . \tag{20}$$

Note that when condition (16) is satisfied, all of the radical expressions in Eqs. (17) and (19) have real values for $\zeta\geq 0$.

The dimensionless electric field is the negative of the derivative of $\Phi(\zeta)$ as given by (17), but a more convenient expression for it may be obtained by differentiating the cubic equation (13). This gives

$$\mathcal{E}(\zeta)=-\frac{d\Phi}{d\zeta}=-\frac{c_1'(\zeta)[1-2\Phi(\zeta)]+c_0'(\zeta)}{6[1-2\Phi(\zeta)]^2+4c_2[1-2\Phi(\zeta)]+2c_1(\zeta)} , \tag{21}$$

$c_1'(\zeta)$ and $c_0'(\zeta)$ being derivatives of the coefficients (15) with respect to ζ.

IV. PARAMETERS FOR N-BODY SIMULATIONS

Direct N-body integration schemes for particles interacting through long-range forces are subject to rather severe limitations on the number of particles that can be followed (see Appendix A for a description of the method used here). In the present context, this fact has two immediate implications.

(i) We can model only a *finite volume* of an infinite plane-parallel sheath; this imposes an artificial upper bound on the length scales over which ion-ion interactions contribute to scattering and relaxation phenomena.

(ii) Simulation particles do not represent individual ions but rather *superparticles,* in which the mass and

charge of many ions are coalesced; the physical consequences of such "lumping" must be accounted for.

These limitations may be compensated for by independently varying the number of particles used and the characteristic dimension of the simulation "control volume" over the greatest practical ranges, and then attempting to extrapolate from such simulations to results that are pertinent to physical values of the parameters.

A. The superparticle factor

In the simulations we employ a cylindrical control volume C whose axis is perpendicular to the cathode. C is of length d, the sheath thickness, and radius a, which may be varied to assess the importance of encounters over increasing length scales. If (r,ϕ,z) and (v_r,v_ϕ,v_z) denote the cylindrical coordinates and velocity components of any particle, its confinement to the volume C may be effected by negating v_r whenever $r>a$. Note that such "reflections" from the control-volume walls have no influence on the polar angle distribution of the ion velocities.

Writing $\delta=d/\lambda_D$ and $\alpha=a/\lambda_D$, the physical number of ions within the control volume is given by

$$N_C=N_D\frac{3\alpha^2}{4}\int_0^\delta \nu(\zeta)d\zeta \ , \tag{22}$$

where ν is the dimensionless density given by Eq. (19) and a numerical quadrature is required. Here we have introduced the *plasma parameter*

$$N_D=\frac{4\pi}{3}\lambda_D^3 n_0 \ , \tag{23}$$

i.e., the total number of electrons in a Debye sphere (at the plasma-sheath boundary). We note that the factor

$$\Omega=\frac{N_C}{N} \tag{24}$$

by which the number N of particles actually used in simulations falls short of (22) indicates the number of ions that have been lumped into each "superparticle." We shall be interested in the extrapolation of results obtained at large values of Ω and finite values of α to the limits $\Omega\to 1$ and $\alpha\to\infty$.

B. Smooth field within the control volume

For particles of charge q_i and mass m_i, the equations of motion are

$$\frac{d^2\mathbf{r}_i}{dt^2}=\frac{q_i}{m_i}\left[\frac{1}{4\pi\epsilon_0}\sum_{j(\neq i)}^{N} q_j\frac{\mathbf{r}_i-\mathbf{r}_j}{|\mathbf{r}_i-\mathbf{r}_j|^3}+\mathbf{E}_S(\mathbf{r}_i)\right] \tag{25}$$

for $i=1,\ldots,N$, where $\mathbf{E}_S(\mathbf{r})$ denotes a smooth field, which is defined as follows.

Although, in terms of monitoring the angular scattering of ions due to discrete Coulomb interactions, we will ignore the mutual repulsions of any pair of ions whose members are not *both* inside the control volume C, it is nevertheless essential to incorporate the influence of the *mean field due to all charges outside of C* upon the trajectories of ions inside it. $\mathbf{E}_S(\mathbf{r})$ represents this smooth field; it counterbalances the tendency of the particles in C, under their mutual repulsions, to deviate in the mean from the longitudinal distribution given by (19) or to develop radial density gradients.

Now by the principle of superposition, we may write

$$\mathbf{E}_S(\mathbf{r})=E(z)\hat{\mathbf{z}}-\mathbf{E}_C(\mathbf{r}) \ , \tag{26}$$

where the first term on the right denotes the modified Child-Langmuir field derived in Sec. III, while $\mathbf{E}_C(\mathbf{r})$ represents the contribution to the former of the smooth charge distribution *inside* the control volume C. Since $\mathbf{E}_C(\mathbf{r})$ is not strictly longitudinal, the field $\mathbf{E}_S(\mathbf{r})$ evidently has a radial component at each location. Note that, in dynamical equilibrium, the N-body term in Eq. (25) becomes identical to $\mathbf{E}_C(\mathbf{r})$ in the limit $N\to\infty$. Thus, for finite N, Eqs. (25) may also be written in the form

$$\frac{d^2\mathbf{r}_i}{dt^2}=\frac{q_i}{m_i}[E(z_i)\hat{\mathbf{z}}+\tilde{\mathbf{E}}(\mathbf{r}_i,t)] \ , \tag{27}$$

representing motion in the smooth longitudinal Child-Langmuir field with a superposed rapidly fluctuating "stochastic" field $\tilde{\mathbf{E}}(\mathbf{r},t)$ of zero mean value (arising from the discrete Coulomb interactions).

We formulate the field $\mathbf{E}_C(\mathbf{r})$ due to the smoothed-out charge distribution *within* the control volume C as the negative gradient of the potential

$$V_C(r,z)=q\int_0^d V_{\rm disk}(r,z-z')n(z')dz' \ , \tag{28}$$

where the function $V_{\rm disk}$ describes, in cylindrical coordinates, the potential due to a uniform disk of unit charge density and radius a, centered on the origin in the plane $z=0$:

$$V_{\rm disk}(r,z)=\frac{1}{4\pi\epsilon_0}\int_0^a\int_{-\pi}^{+\pi}\frac{r'd\varphi\,dr'}{\sqrt{r'^2-2rr'\cos\varphi+r^2+z^2}} \ . \tag{29}$$

The evaluation of the integral (29) is described in Appendix B.

With $(\rho,\zeta)=(r/\lambda_D,z/\lambda_D)$, the dimensionless form of Eq. (28) is

$$\Phi_C(\rho,\zeta)=\frac{1}{4\pi}\int_0^\delta \Phi_{\rm disk}(\rho,\zeta-\zeta')\nu(\zeta')d\zeta' \ , \tag{30}$$

where

$$\Phi_{\rm disk}(\rho,\zeta)=\epsilon_0\lambda_D^{-1}V_{\rm disk}(\lambda_D\rho,\lambda_D\zeta)$$

and $\nu(\zeta)$ is the dimensionless ion density given by Eq. (19). The complicated form of the integrand in (30) means that $\Phi_C(\rho,\zeta)$ must be computed numerically. However, it will be very inefficient to perform this quadrature at the current position of a particle each time it is to be stepped. Since $\Phi_C(\rho,\zeta)$ is a smoothly varying function, it may be described to high accuracy by evaluating it just *once* on a suitable grid of $m\times n$ locations (ρ_j,ζ_k) within the control volume and using a C^2 bicubic "tensor-product" spline to interpolate for intermediate values.

Thus, writing $\Delta\rho=\alpha/m$ and $\Delta\zeta=\delta/n$, we use the approximation

$$\Phi_C(\rho,\zeta)=\sum_{j=0}^{m}\sum_{k=0}^{n}\Phi_{jk}R_j(\rho)Z_k(\zeta)\ , \tag{31}$$

where $\Phi_{jk}=\Phi_C(\rho_j,\zeta_k)$ denotes the true potential at location $(j\Delta\rho,k\Delta\zeta)$, obtained by explicit evaluation of (30). The radial and longitudinal spline bases $\{R_j(\rho)\}$ and $\{Z_k(\zeta)\}$ used in (31) are C^2 piecewise-cubic functions [22] satisfying the interpolatory conditions

$$R_j(i\Delta\rho)=\delta_{ij}\quad\text{and}\quad Z_k(l\Delta\zeta)=\delta_{kl} \tag{32}$$

for $0\le i,\ j\le m$ and $0\le k,\ l\le n$. As end conditions, we employ quadratic end spans, except for the radial basis at $\rho=0$, where the condition $R_j'(0)=0$ for $j=0,\ldots,m$ is imposed to ensure that particles on the symmetry axis of the control volume C experience no radial force due to $\mathbf{E}_S(\mathbf{r})$.

The smooth force field $\mathbf{E}_S(\mathbf{r})$ within the control volume C is illustrated in Fig. 1 for two different aspect ratios of C, using the density distribution (19) with $\mathcal{E}_0=1$. Note that the radial component of $\mathbf{E}_S(\mathbf{r})$ is always negative, counteracting the tendency of the simulation particles within C to diffuse radially outward under their mutual repulsions.

C. Use of "softened" forces

Writing $\xi_i=\mathbf{r}_i/\lambda_D$ and $\tau=\omega_p t$, and assuming superparticles of equal mass $m_i=\Omega m$ and charge $q_i=\Omega q$ for $i=1,\ldots,N$, the dimensionless form of the equations of motion (25) becomes

$$\frac{d^2\xi_i}{d\tau^2}=\Gamma_N\sum_{j\,(\neq i)}^{N}\frac{\xi_i-\xi_j}{|\xi_i-\xi_j|^3}+\mathcal{E}_S(\xi_i) \tag{33}$$

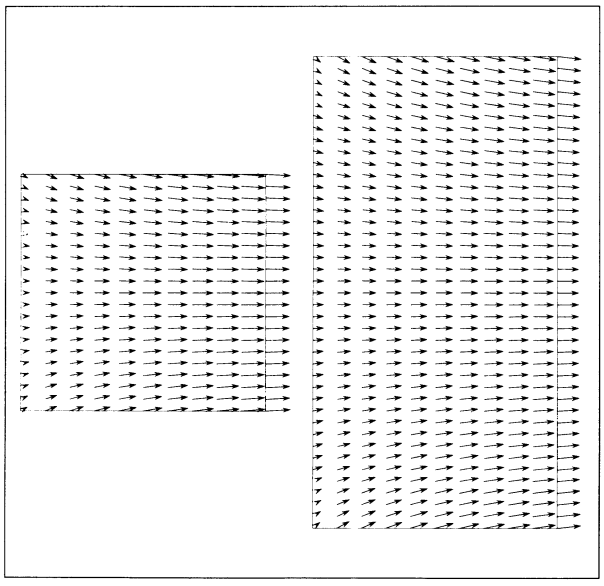

FIG. 1. Variation of the smooth force field $\mathbf{E}_S(\mathbf{r})$ given by Eq. (26) over an axial cross section of the cylindrical control volume C, for two values of the aspect ratio $2\alpha/\delta$.

for $i=1,\ldots,N$, where

$$\mathcal{E}_S(\xi)=(q\lambda_D/mu_0^2)\mathbf{E}_S(\mathbf{r}/\lambda_D)$$

and the "coupling constant" for the N-body term,

$$\Gamma_N=\frac{\Omega}{3N_D}=\frac{N_C/N_D}{3N}\ , \tag{34}$$

is proportional to the superparticle factor (24) and inversely proportional to the plasma parameter (23). The second form for Γ_N given above arises from Eq. (24) and illustrates that $\Gamma_N\propto N^{-1}$ for fixed physical sheath parameters ($N_C/N_D=$const) [see Eqs. (22) and (23)].

As a computational convenience, the singularities of the Coulomb forces in Eqs. (33) may be eliminated by "softening" the interaction at small distances—for example, by modifying the denominator of the jth particle contribution to the N-body sum in (33) to

$$[|\xi_i-\xi_j|^2+\sigma_i^2+\sigma_j^2]^{3/2}\ . \tag{35}$$

This corresponds to the interparticle potential

$$\Phi_{ij}\propto[|\xi_i-\xi_j|^2+\sigma_i^2+\sigma_j^2]^{-1/2}$$

instead of $\Phi_{ij}\propto|\xi_i-\xi_j|^{-1}$. The *softening parameters* σ_i may be regarded as finite "radii" of the particles, over which their charges are distributed.

Note that the "softened" interactions are virtually indistinguishable from ordinary Coulomb forces at distances large compared to the particle radii. For physical systems in which close-range encounters play an insignificant role—such as the ion flux in a sheath—the use of softened forces does not materially alter the simulation results (we verify this empirically below). Furthermore, manipulating the values of the softening parameters allows an "effective" value for the minimum impact parameter $b_{\min}$, appropriate to the sheath context, to be directly measured—in lieu of expression (4). Unless otherwise stated, we employ a uniform value $\sigma=0.01$ in every run, this being a small fraction of the mean interparticle spacing in all regimes.

V. RESULTS OF SIMULATIONS

In any simulation, particles initially have longitudinal positions and velocities satisfying the modified Child-Langmuir profiles (19); they have no transverse velocity components, and their radial distribution is uniform. The orientation of each particle velocity vector is recorded upon arrival at the cathode; for each particle absorbed at the cathode, we introduce a new one at the plasma-sheath boundary—this emulates a uniform flux and ensures that the total particle number N remains constant during the simulation.

We record only those particles received at the cathode that have made a full sheath traversal. Upon replacing any particle at the cathode by one at the plasma-sheath boundary, the integration scheme is "restarted" so as to minimize errors that would otherwise be induced by discontinuities in the force field due to the sudden appearance and disappearance of particles. This means that all the particles must be synchronized (see Appendix A),

affording an opportunity to sample their global distribution for the purpose of computing time-averaged density, velocity, and mean-field profiles.

Since we cannot afford to explore the parameter space defining the sheath structure in much detail, we choose a "canonical" case about which only a single parameter will be varied in a given sequence of runs. The nominal physical model for this case is the time-average sheath of an O_2 rf discharge, with assumed sheath thickness $d=2$ mm, a gas pressure and temperature of 5 mTorr and 350 K, electron temperature $T_e=10^5$ K, and ionization fraction $f_i=5\times10^{-4}$—the plasma parameter (23) is then $N_D=1.67\times10^5$. In the canonical case we take $a=1$ mm for the radius of the control volume.

In dimensionless terms, the control-volume size is given by $\delta=2\alpha\approx23.9$, while the potential drop across the sheath is $|\Phi(\delta)|\approx90.2$ (the electric field at the plasma-sheath boundary is assumed to be $\mathcal{E}_0=1$). The superparticle factor is then $\Omega=7.31\times10^7N^{-1}$. To achieve uniform sampling in a sequence of runs with different particle numbers, the duration of each run—excluding the initial "settling" period—is taken to be inversely proportional to N.

A. Verification of dynamical equilibrium

The deviations of the ion motions from the continuum description of Sec. III that we wish to monitor are quite subtle, so it is important to establish that the simulation scheme does indeed agree with the modified Child-Langmuir model in the mean. Figure 2 compares the time-averaged sheath structure, determined from the particle distributions, with the Child-Langmuir model in a typical case. The agreement is seen to be very good, although the statistics are much better for longitudinal profiles than radial ones since, on traversing the sheath, a particle may be sampled at each longitudinal coordinate, whereas its radial coordinate is roughly constant.

We have also monitored the time-average electric field (due to the smooth component $\mathcal{E}_S$ and the fluctuating contribution of the N particles) in the control volume. No systematic deviation of this mean field from the strictly longitudinal Child-Langmuir form could be discerned; the residual vector difference was found to have a magnitude that decreased continuously with the sampling frequency and an orientation varying randomly with location.

B. Dependence of $\theta_{\rm rms}$ on Ω

The simulation particles experience a stochastic field whose "graininess" is enhanced by the superparticle factor Ω over that in a physical sheath. Thus, we need to investigate the rate at which the angular dispersion of the ion flux diminishes as this factor is reduced toward the physical limit $\Omega=1$.

For reasons that will become apparent in Sec. VI, we prefer to characterize the angular dispersion by the root-mean-square polar angle $\theta_{\rm rms}=\sqrt{\langle\theta^2\rangle}$ of the ion velocities upon arrival at the cathode, rather than the mean $\langle\theta\rangle$. In any case, the difference between $\theta_{\rm rms}$ and $\langle\theta\rangle$ is generally quite small.

Figure 3 shows, on a log-log plot, the measured dependence of $\theta_{\rm rms}$ on Ω for a sequence of 11 runs in which the particle number N is uniformly increased through the values 12,25,50,100,...,12 800, all other quantities being held constant. The "error bars" shown here (and, unless otherwise stated, in all subsequent plots of this form) indicate the *spread* of the angular distributions; they represent "one-sided" standard deviations, for angles less than and greater than $\theta_{\rm rms}$ (see Fig. 4). They should *not* be construed as measures of the uncertainty in $\theta_{\rm rms}$, which is typically much smaller.

The dashed line represents a least-squares fit to the data, extended to the physical limit $\Omega=1$. This extrapolation is not incredible, since the available data are remarkably linear and cover more than three decades in Ω, while less than four additional decades are required to attain the desired limit. No new physical effects are expected to arise as Ω is continuously reduced.

For the canonical sheath model, we infer that the physical ion flux at the cathode has an angular distribution characterized by $\theta_{\rm rms}\approx0.06°$ (considering only interactions on length scales not exceeding the sheath thickness and assuming a perfectly "cold" ion flux at the plasma-sheath boundary). This is probably below current experimental resolution, although it is not utterly negligible. Different values of the sheath parameters can give rise to greater angular dispersions (see Sec. V E below).

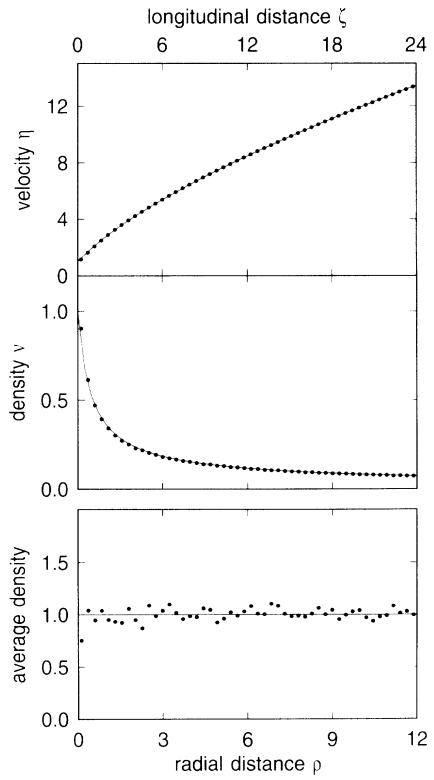

FIG. 2. Comparison of time-averaged profiles (dots) for the particle stream velocity and number density obtained in a typical run with the modified Child-Langmuir profiles (smooth curves) defined by Eq. (19).

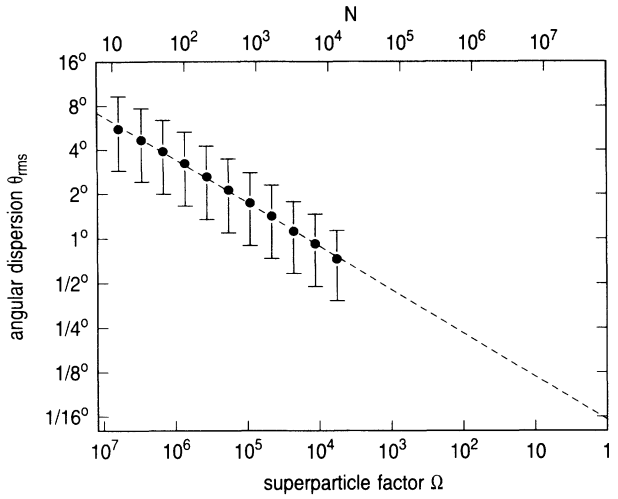

FIG. 3. Dependence of the scattering angle θ_{rms} on the superparticle factor Ω for a series of simulations using an increasing number N of particles, with all other parameters held constant (note that both axes are logarithmic). The dashed line represents a least-squares fit to the available data, extended to the physical limit $\Omega=1$.

The data of Fig. 3 are consistent with a power-law relation $\theta_{rms} \propto \Omega^k$, the exponent estimated from the least-squares fit being $k=0.294\pm0.004$. This relation is significantly weaker than the $\sqrt{\Omega}$ scaling that naive statistical arguments might suggest, indicating the importance of nonlinear effects. We will attempt to explain the measured value of k in Sec. VI below.

C. Empirical determination of b_{min}

For large-N Coulomb systems, it is commonly understood that the numerous small deflections due to distant interactions will have a greater cumulative scattering effect than infrequent close approaches [1,2]; we may expect this to be especially true for repulsive systems of like-sign charges, such as the ion flux in a sheath. Furthermore, in order to avoid a divergence of quantities that incur an integration over impact parameters—such as the dynamical-friction and velocity-diffusion coefficients (1) and (2)—a finite lower bound b_{min} must be imposed on the range of interactions considered.

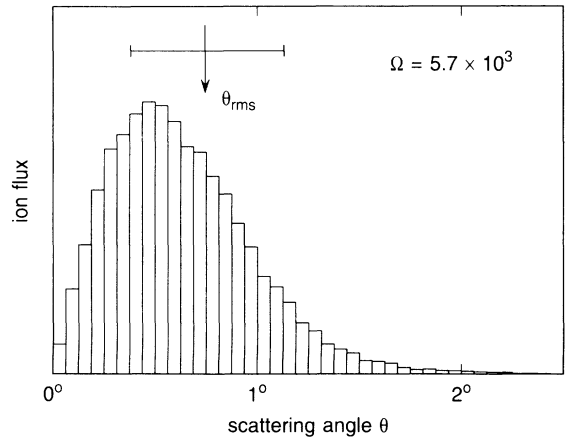

FIG. 4. Angular distribution of ions incident on the cathode in a typical case. The location of the root-mean-square value θ_{rms}, and the angular "spread" (defined by one-sided standard deviations) about θ_{rms}, are shown.

Using the Landau length quoted in Eq. (4) for b_{min} is not justified in the present context, since the ion gas in the sheath is far from thermal equilibrium and cannot usefully be characterized by a temperature T. However, desingularizing the Coulomb forces by introducing softening parameters [see Eq. (35) above] allows us to directly measure an "effective" value for b_{min} by observing when, as the finite particle size is increased, it begins to influence the angular distribution measured at the cathode.

In the present context, we find that b_{min} can be accurately characterized as a fraction f of the mean interparticle spacing $l_0=(\Omega^{-1}n_0)^{-1/3}$ *at the plasma-sheath boundary.* In dimensionless terms, we write

$$\beta_{min}=\frac{b_{min}}{\lambda_D}=f\left[\frac{4\pi}{3}\frac{\Omega}{N_D}\right]^{1/3} \tag{36}$$

as the lower cutoff appropriate to any given simulation, with the unique coefficient f to be determined empirically. Figure 5 shows data for runs with $N=100$ and 1600:

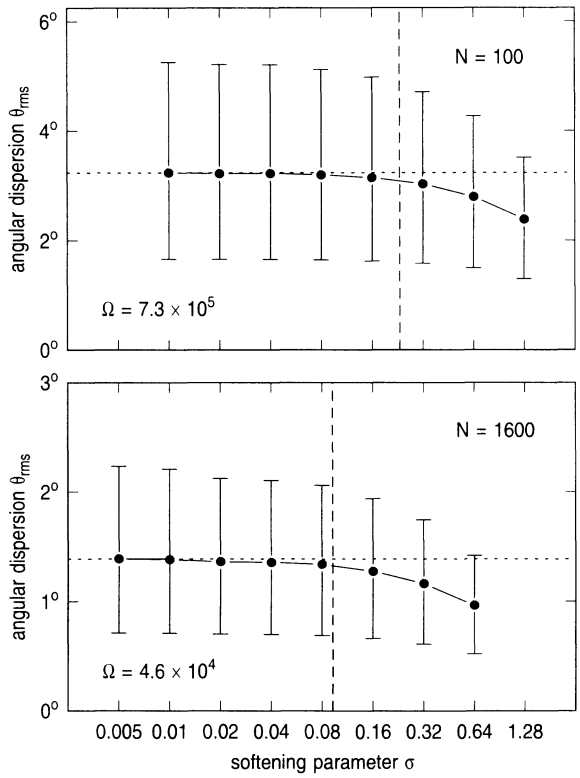

FIG. 5. Dependence of the scattering angle θ_{rms} on the softening parameter σ for two runs with different particle numbers. Note that θ_{rms}, as well as the angular spread indicated by the "error" bars, is essentially constant when $\sigma<\beta_{min}$, the value adopted in Eq. (36) for the lower bound in the Coulomb logarithm (indicated here by the dashed line).

In both cases we see that, when the softening radius σ is reduced below some threshold value (which may be identified with $\beta_{\min}/\sqrt{2}$), $\theta_{\rm rms}$ and the angular spread asymptote to unique values.

The dashed lines in Fig. 5 indicate the values $\sigma=\beta_{\min}/\sqrt{2}$ with the choice $f=\frac{1}{8}$ in (36). While there is some ambiguity in the precise location of the threshold that determines $\beta_{\min}$, it amounts to no more than a factor of 2, corresponding to an insignificant uncertainty in the value of $\ln\Lambda$.

[Note that if the softening parameter σ is increased too far and becomes comparable to the mean interparticle spacing at any location, it will begin to compromise the capacity of the particles to exert a mean field that accurately compensates the term $\mathbf{E}_C(\mathbf{r})$ in Eq. (26). The ideal of Eq. (27)—corresponding to motion in a stochastic, zero-mean field $\tilde{\mathbf{E}}(\mathbf{r},t)$ superposed on the smooth, longitudinal Child-Langmuir field $E(z)$—is then no longer realized, and measurements of the angular distribution cannot be trusted because systematic radial field components begin to develop. This artifact is manifested by a sudden upturn of the scattering angle $\theta_{\rm rms}$ if one attempts to extend the data of Fig. 5 to larger σ values.]

The fact that $\beta_{\min}$ is determined by the mean interparticle spacing *at the plasma-sheath boundary*—where the ion density is highest—is consistent with arguments that will be presented in Sec. VI below.

D. Search for a bound on $b_{\max}$

We have attempted to investigate the influence of Coulomb interactions over increasing length scales by expanding the radius of the control volume C with all other parameters held fixed. Unfortunately, the dynamic range in the aspect ratio $2\alpha/\delta$ that can be explored is very limited since, for fixed Ω, doubling α incurs a *fourfold* increase in the particle number N.

(Note that, for a given α, our model slightly *underestimates* the overall effect of interactions on length scales α in the transverse direction. Whereas a particle traversing the control volume C along its axis will be surrounded by other particles at distances up to α in all transverse directions, one whose trajectory lies near the periphery of C will experience a weaker stochastic field since particles outside C have been replaced by the smooth field $\mathcal{E}_S$.)

Figure 6 shows, in the usual manner, the observed dependence of $\theta_{\rm rms}$ on the control-volume aspect ratio $2\alpha/\delta$ over a dynamic range of just 16. To keep Ω fixed, the particle number N must be increased so as to maintain, from run to run, a fixed mean density at each longitudinal distance into the sheath. Even if we begin with the small value $N=25$ at $2\alpha/\delta=1$, it is difficult to extend the data much beyond one decade in the aspect ratio.

Since the variation of $\theta_{\rm rms}$ seen in Fig. 6 is quite subtle, some numerical values are provided in Table I together with estimates of their uncertainties—based on sampling a total of $\sim 12\,800$ ion traversals in each run. There is an incontrovertible increase in $\theta_{\rm rms}$ as Coulomb interactions over an increasing lateral extent are taken into account. Thus, taking $\beta_{\max}=\delta$ in $\ln\Lambda$ would definitely *underestimate* somewhat the overall angular dispersion of the ion flux in typical sheath contexts.

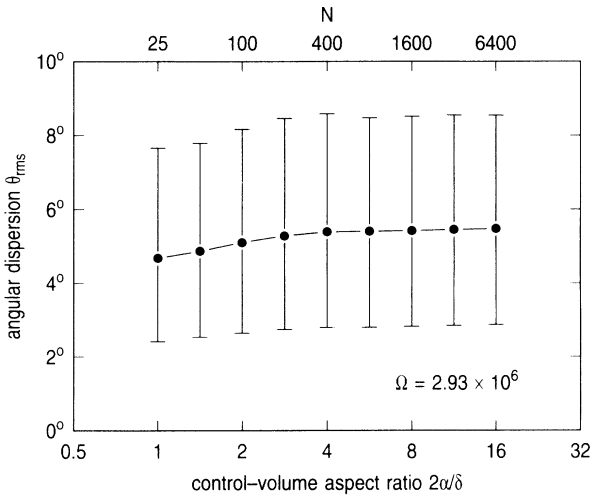

FIG. 6. Dependence of the scattering angle $\theta_{\rm rms}$ on the logarithm of the control-volume aspect ratio $2\alpha/\delta$.

Since theoretical arguments (see Sec. VI) suggest that the *mean-square* angle $\langle\theta^2\rangle=\theta_{\rm rms}^2$ should grow in proportion to $\ln\Lambda$, we plot this quantity in Fig. 7 against the logarithm of $2\alpha/\delta$ on a greatly magnified scale, with error bars reflecting the estimated uncertainty of each value. Evidently, $\langle\theta^2\rangle$ does not continue to grow linearly with $\ln(2\alpha/\delta)$—we observe a definite asymptotic tendency, suggesting that a finite "effective" upper cutoff $\beta_{\max}$ exists.

It is not essential to assume that $\beta_{\max}\propto\alpha$ in order to infer a finite upper cutoff from Fig. 7. One might also postulate that $\beta_{\max}$ grows like the *geometric mean* $(\alpha^2\delta)^{1/3}$ of the transverse and longitudinal dimensions, but this also predicts a (somewhat slower) linear increase of $\theta_{\rm rms}^2$ with $\ln(2\alpha/\delta)$. Perhaps the main conclusion to be drawn from Figs. 6 and 7 is that, even in the absence of Debye screening, a sustained logarithmic growth of scattering and relaxation phenomena with the system dimensions is *not* achieved.

Unfortunately, the available data are insufficient in quality and extent to draw any definitive conclusions regarding the upper cutoff in the Coulomb logarithm. For practical purposes, however, if we split $\ln\Lambda$ up as

$$\ln\Lambda=\ln\frac{\beta_{\max}}{\delta}+\ln\frac{\delta}{\beta_{\min}}\ , \tag{37}$$

with $\beta_{\min}$ given by (36), the simulations suggest that the argument of the first logarithm should be no more than

TABLE I. Variation of $\theta_{\rm rms}$ with $2\alpha/\delta$.

Aspect ratio	Angular dispersion
1	4.683°±0.042°
2	5.114°±0.046°
4	5.397°±0.048°
8	5.431°±0.048°
16	5.485°±0.049°

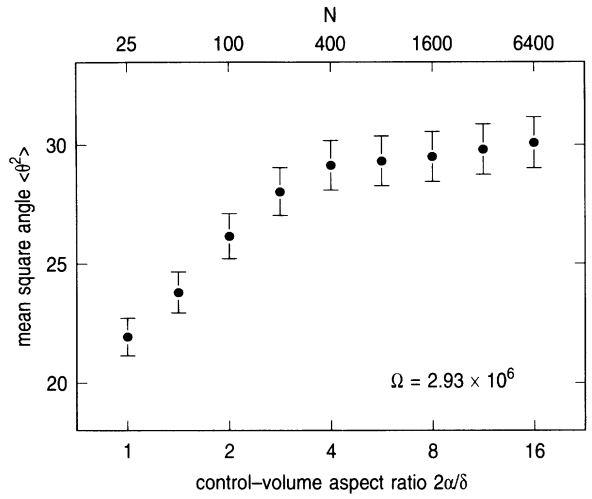

FIG. 7. The mean-square polar angle $\langle\theta^2\rangle = \theta^2_{\rm rms}$ of ion velocities at the cathode plotted against the logarithm of the aspect ratio on a magnified scale. Here the error bars represent uncertainties in $\langle\theta^2\rangle$ due to the sampling statistics, not the spread of the angular distribution.

~ 10. In that case, the contribution of the second term will invariably dominate in the limit $\Omega \to 1$.

The behavior seen in Fig. 7 is consistent with the notion that a form of Debye screening occurs even in a "non-neutral plasma," consisting of a single species of particles of like charge in dynamical equilibrium with their own space-charge field and external fields [23].

E. Dependence of $\theta_{\rm rms}$ on sheath parameters

Finally, we examine how various physical properties of the sheath influence the angular dispersion $\theta_{\rm rms}$. The principal physical parameters characterizing the sheath are the ion current density $J = qn_0u_0$ across the sheath and the sheath thickness $d = \lambda_D\delta$ and potential $V = -mu_0^2\Phi(\delta)/q$. Only two of these quantities may be independently varied—they are related, in a rather complicated manner, by the model of Sec. III. In most cases the classical Child-Langmuir law [24,25]

$$J^2 \approx \frac{32q\epsilon_0^2V^3}{81md^4} \tag{38}$$

is a good approximation. For brevity, we shall confine our attention here to independently varying the sheath thickness d and the plasma density n_0.

A sequence of runs corresponding to the values $\delta \approx 6, 12, 18, \ldots, 48$ of the dimensionless sheath thickness was performed, with all other quantities held fixed. Note that the potential drop $|\Phi(\delta)|$ across the sheath increases monotonically with δ, as determined by Eq. (17). In order to keep the superparticle factor Ω constant, the actual number N of simulation particles used from run to run was made proportional to the integral (22).

Since the ion stream velocity increases by a factor $\sqrt{1-2\Phi(\delta)}$ across the sheath, we should expect that $\theta_{\rm rms}$ will decrease as δ—and hence $|\Phi(\delta)|$—is increased. Figure 8(a) shows, consistent with this expectation, the measured values of $\theta_{\rm rms}$ against δ. To compare with the theory outlined in Sec. VI, we also show in Fig 8(b) the variation of $\theta_{\rm rms}$ with the ultimate stream velocity $\eta(\delta)$ on a log-log plot. The least-squares fit of $\log_{10}\theta_{\rm rms}$ against $\log_{10}\eta(\delta)$ yields a slope of -1.010 ± 0.019, giving an accurate indication that $\theta_{\rm rms}$ diminishes in inverse proportion to $\eta(\delta)$.

In another sequence of runs, we have studied the dependence of $\theta_{\rm rms}$ on the plasma density n_0. In order to keep the potential drop $|\Phi(\delta)|$ constant, the sheath thickness δ (measured in Debye lengths) must remain fixed. Since $\lambda_D \propto n_0^{-1/2}$, this means that the physical dimensions of the control volume decrease as we increase n_0 (the aspect ratio is also held fixed at $2\alpha/\delta = 1$). From Eqs. (22)–(24) we then see that the particle number must be chosen to satisfy $N \propto N_D \propto n_0^{-1/2}$ if Ω is to remain unchanged from run to run.

Since the variation of $\theta_{\rm rms}$ with n_0 is relatively weak, we double the plasma density between consecutive runs. As illustrated in Fig. 9(a), there is a systematic increase of $\theta_{\rm rms}$ with the logarithm of n_0. In Fig. 9(b) we also show, on a log-log plot, the variation of $\theta_{\rm rms}$ with the plasma parameter N_D ($\propto n_0^{-1/2}$). From a least-squares fit we find that $\theta_{\rm rms} \propto N_D^{-0.316 \pm 0.007}$, which agrees reasonably well with the theory presented below.

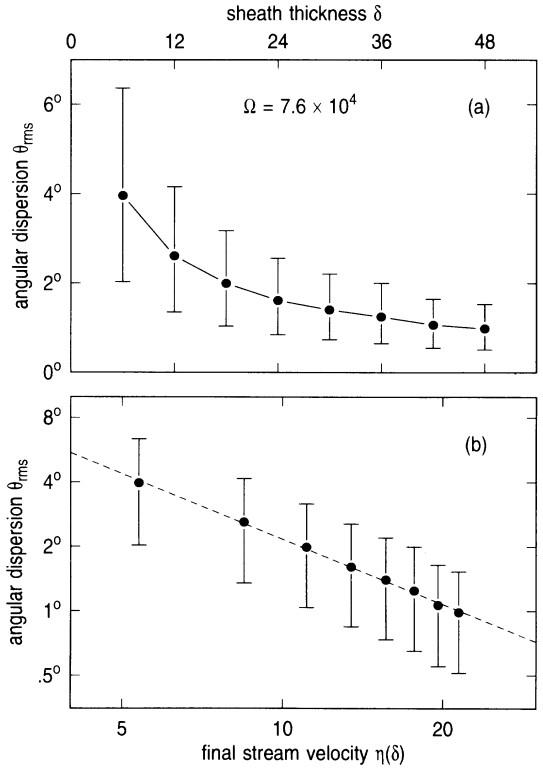

FIG. 8. (a) Angular dispersion $\theta_{\rm rms}$ vs the sheath thickness δ for a series of runs with the superparticle factor Ω held constant. (b) A log-log plot of $\theta_{\rm rms}$ against the final stream velocity $\eta(\delta) = \sqrt{1-2\Phi(\delta)}$ for the same sequence of runs; the dashed line represents a least-squares fit.

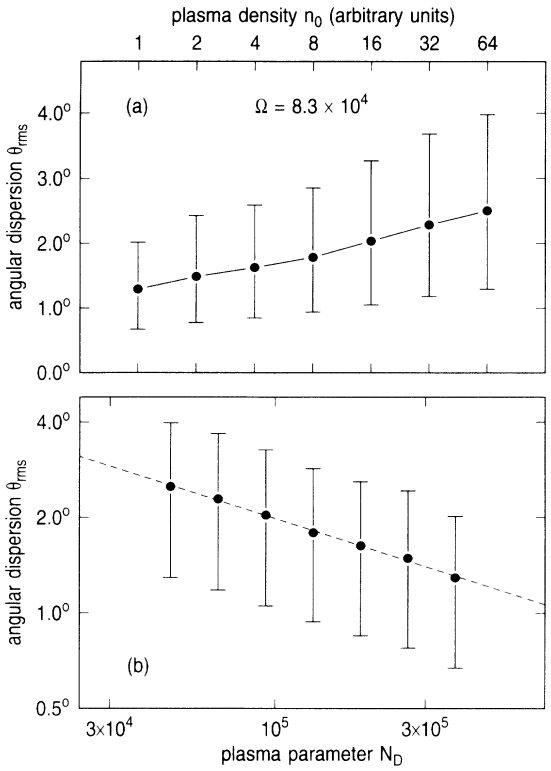

FIG. 9. (a) Angular dispersion $\theta_{\rm rms}$ vs the logarithm of the plasma density n_0 for a series of runs with Ω constant. (b) A log-log plot of $\theta_{\rm rms}$ against the plasma parameter N_D defined by Eq. (23) for the same sequence of runs; the dashed line is a least-squares fit.

VI. COMPARISON WITH DIFFUSION THEORY

In Sec. II we noted several arguments *against* making use of the Chandrasekhar "dynamical-friction" and "diffusion" coefficients (1) and (2) in the present context. Nevertheless, if we temporarily suspend these arguments and apply expressions (1) and (2) regardless, a plausible explanation for the exponent $k \approx 0.294$ in the $\theta_{\rm rms} \propto \Omega^k$ law discussed in Sec. V B can be identified.

The transverse coefficient $\langle (\Delta v_\perp)^2 \rangle$ is the quantity of principal interest, since, over the sheath extent, the fractional changes that $\langle \Delta v_\parallel \rangle$ and $\langle (\Delta v_\parallel)^2 \rangle$ incur in the final ion stream velocity are small and have a negligible influence on $\theta_{\rm rms}$. Now the appropriate speed v of the "test" particle to be used in expression (2) is *not* the stream velocity $u(z)$ given (in units of u_0) by (19), since the background "field" particles are also moving at this speed—we are confronted again with the dilemma that test particles are also field particles; the speed of the former relative to the latter is not unambiguously defined.

We can circumvent this problem by applying expressions (2) *in a reference frame moving with the local stream velocity.* In such a frame, a "test" particle is typically stationary ($v=0$) relative to the background, whereas the "field" particles have random motions which define the background "temperature." It must be admitted, of course, that the adopted frame is *noninertial*—it accelerates at a rate determined by the Child-Langmuir field—while the Chandrasekhar theory described in Sec. II is specific to inertial frames.

We will not attempt a rigorous justification for our current usage. The rederivation of expressions (1) and (2) for noninertial frames is a formidable task, beyond our present scope. As we shall presently see, the effects that concern us occur primarily within a few Debye lengths of the plasma-sheath boundary, where the field is relatively weak. Also, noninertial corrections to the transverse coefficient $\langle (\Delta v_\perp)^2 \rangle$ are expected to be less important than those to $\langle \Delta v_\parallel \rangle$ or $\langle (\Delta v_\parallel)^2 \rangle$, which measure changes in the field direction.

Noting that $x^2 = mv^2/2kT$ in expressions (1) and (2), it may be verified by use of L'Hôpital's rule that for a test particle at rest ($v=0$) the velocity-diffusion coefficients have the limiting values

$$\lim_{v\to 0} \langle (\Delta v_\perp)^2 \rangle = 2 \lim_{v\to 0} \langle (\Delta v_\parallel)^2 \rangle = \frac{4q^4 n \ln\Lambda}{3(2\pi)^{3/2}\epsilon_0^2 m^2} \left[\frac{m}{kT}\right]^{1/2} , \tag{39}$$

while the dynamical-friction coefficient $\langle \Delta v_\parallel \rangle$ vanishes in this limit (the above also represent *bounds* on the diffusion coefficients, for any value of $mv^2/2kT$, so the arguments that follow may alternately be regarded as establishing a bound on the angular dispersion).

Now in general we may expect to find different "temperatures,"

$$kT_\perp = \tfrac{1}{2} m \langle v_x^2 + v_y^2 \rangle \quad \text{and} \quad kT_\parallel = m \langle (v_z - u)^2 \rangle , \tag{40}$$

in the longitudinal and transverse directions. We assume that the value to be used on the right-hand side of (39) is the mean, $T = \frac{2}{3} T_\perp + \frac{1}{3} T_\parallel$. With the definitions (40), we can identify expression (39) as the rate at which $2kT_\perp/m$ or $2kT_\parallel/m$ increases with time. Thus, writing $d/dt = u\, d/dz$, we have

$$\frac{d}{dz}\frac{kT_\perp}{m} = \frac{d}{dz}\frac{kT_\parallel}{m} = \frac{2q^4 n \ln\Lambda}{3(2\pi)^{3/2}\epsilon_0^2 m^2 u} \left[\frac{m}{kT}\right]^{1/2} , \tag{41}$$

and assuming $T_\perp = T_\parallel = 0$ at $z=0$, it follows from the above that $T_\perp(z) \equiv T_\parallel(z) \equiv T(z)$. Since n and u are known functions of z, (41) amounts to a first-order, nonlinear equation that determines the *unique* temperature $T(z)$ as a function of distance into the sheath.

To cast Eq. (41) in a dimensionless form appropriate for comparison with the simulations, we write $kT/m = u_0^2 \Theta$ and then replace q, m, n, u, and z by Ωq, Ωm, $\Omega^{-1} n_0 \nu$, $u_0 \eta$, and $\lambda_D \zeta$. After simplification, this gives

$$\frac{d\Theta}{d\zeta} = \frac{4}{9\sqrt{2\pi}} \frac{\Omega}{N_D} \frac{\nu^2 \ln\Lambda}{\sqrt{\Theta}} , \tag{42}$$

where N_D is the plasma parameter given by (23), and we have used the fact that $\nu(\zeta)\eta(\zeta) \equiv 1$ by conservation of the ion flux.

Assuming $\Theta = 0$ at $\zeta = 0$ and taking $\ln\Lambda$ to be roughly

constant, we may integrate Eq. (42) to obtain the temperature profile

$$\Theta(\xi)=\left[\frac{2}{9\pi}\right]^{1/3}\left[\frac{\Omega}{N_D}\ln\Lambda\int_0^{\xi}\nu^2(\xi')d\xi'\right]^{2/3} \tag{43}$$

within the sheath. Note that, since the density ν falls rapidly with distance ξ (see Fig. 2), we expect according to (43) that Θ will rise quickly in the first few Debye lengths but then show little further increase (see Fig. 10).

Figure 11 illustrates representative time-averaged profiles for the particle temperatures defined by Eq. (40). While the behavior suggested by expression (43) can clearly be seen, a significant departure from the above model is also evident: The residual particle motions about the stream velocity are strongly anisotropic, with $T_{\parallel}\ll T_{\perp}$. The source of this discrepancy is uncertain; it may be that the tranverse diffusion coefficient holds reasonably well in a noninertial frame, whereas the longitudinal one does not.

Henceforth, we shall identify Θ with $kT_{\perp}/mu_0^2$, since it is the transverse temperature that determines the angular dispersion $\theta_{\rm rms}$. As noted above, this temperature is built up mostly near $\xi=0$ because (i) there is a higher density of "field" particles in this region and (ii) a "test" particle spends more time there, since the stream velocity is smaller.

In Fig. 12 we show the dependence of the "asymptotic" temperatures—measured at $\xi\gg1$—on the superparticle factor Ω. Equation (43) predicts $T_{\perp}\propto\Omega^{2/3}$, while a least-squares fit to the data shown gives $T_{\perp}\propto\Omega^{0.626\pm0.019}$. While the weak dependence of $\ln\Lambda$ on Ω through expression (36) accounts for a small part of the difference, it is sufficiently large for one to suspect that systematic corrections to $\langle(\Delta v_{\perp})^2\rangle$ are required in a noninertial frame. Nevertheless, in view of the simplifying assumptions one might also regard this as a very good agreement. For the longitudinal temperature, the least-squares fit gives $T_{\parallel}\propto\Omega^{0.505\pm0.008}$, which does not agree well with (43).

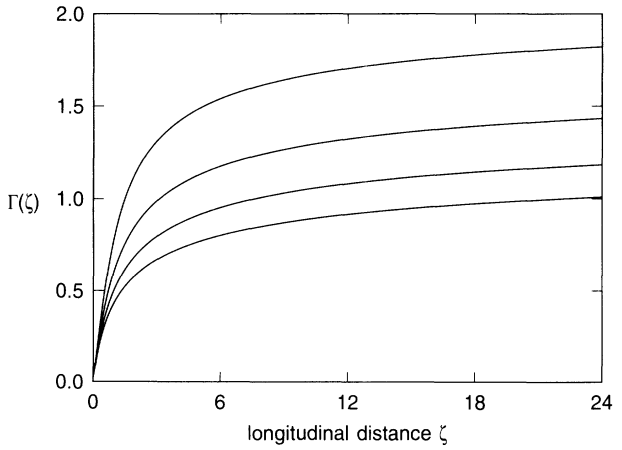

FIG. 10. The integral $\Gamma(\xi)$ of the square of the dimensionless ion density $\nu(\xi)$ that occurs in the temperature profile (43) for values $\mathcal{E}_0=0.0$, 0.5, 1.0, and 1.5 of the initial field (from top to bottom).

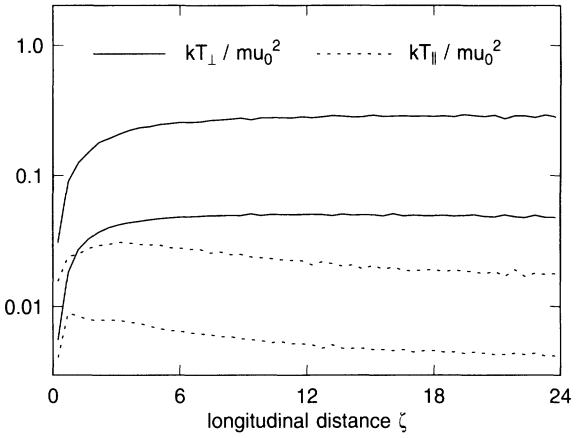

FIG. 11. Time-averaged profiles of the longitudinal and transverse particle temperatures $T_{\parallel}$ and $T_{\perp}$, given by Eq. (40), for runs with $N=100$ ($\Omega=7.3\times10^5$) and $N=1600$ ($\Omega=4.6\times10^4$); the higher curves are for the larger value of Ω.

Finally, we turn to the measured dependence of the angular dispersion $\theta_{\rm rms}$ on the superparticle factor Ω shown in Fig. 3 and discussed in Sec. V B. Identifying expression (43) with $kT_{\perp}/mu_0^2$ and noting that

$$\theta_{\rm rms}\approx\frac{v_{\perp,\rm rms}}{u(d)}\ , \tag{44}$$

where $v_{\perp,\rm rms}=\sqrt{2kT_{\perp}/m}$ and $u(d)$ denote the root-mean-square transverse velocity and the stream velocity at the cathode, we obtain

$$\theta_{\rm rms}\approx\left[\frac{16}{9\pi}\right]^{1/6}\frac{1}{\eta(\delta)}\left[\frac{\Omega}{N_D}\ln\Lambda\int_0^{\delta}\nu^2(\xi)d\xi\right]^{1/3}. \tag{45}$$

The empirically determined relation $\theta_{\rm rms}\propto\Omega^{0.294}$ previously quoted in Sec. V B is in fair agreement with the above prediction based on diffusion theory. The error ±0.004 in the empirical exponent, determined from the least-squares fit, clearly cannot account for its deficiency

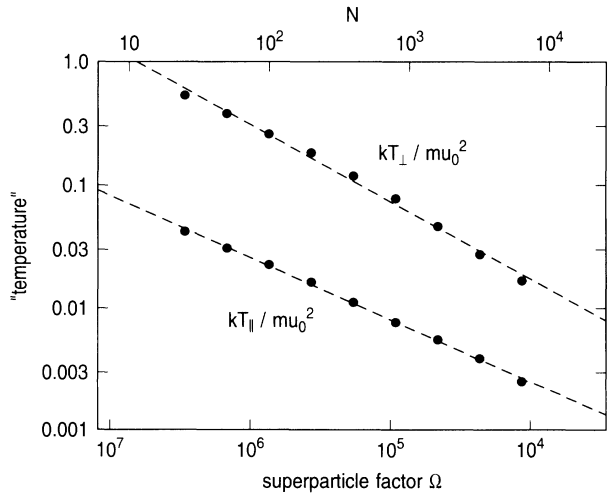

FIG. 12. Dependence of the "asymptotic" longitudinal and transverse temperatures on the superparticle factor Ω (both axes are logarithmic).

compared to the predicted exponent in expression (45). Again, this may be attributed in part to the $\ln\Lambda$ factor, although other systematic effects must be primarily responsible.

The scaling behavior of $\theta_{\rm rms}$ with $\eta(\delta)$ and N_D predicted by expression (45) is also seen to be in good agreement with the results presented in Sec. V E where the sheath thickness and plasma density were varied. Apart from elucidating the observed scaling relationships, however, Eq. (45) should not be expected to give accurate quantitative agreement with the simulation results. In addition to the many simplifications invoked in deriving (45), one may note that since the superparticle factor is quite large ($10^4 \lesssim \Omega \lesssim 10^7$), the difference between its measured exponent of 0.294 ± 0.004 and the value $\frac{1}{3}$ in (45) is alone sufficient to cause appreciable differences.

Note that for physical sheaths ($\Omega = 1$) the plasma parameter N_D assumes the role of the superparticle factor in the simulations, in terms of characterizing the "graininess" of the sheath field. In other words, reducing N_D by a given factor has the same effect on $\theta_{\rm rms}$ as increasing Ω by the same factor. Since $N_D \propto n_0^{-1/2}$ if u_0 (i.e., the electron temperature T_e) is held constant, expression (45) indicates a very weak dependence on the plasma density: $\theta_{\rm rms} \propto n_0^{1/6}$. This is consistent with the data shown in Fig. 9(a).

VII. DISCUSSION

A few qualifications regarding the application of the above results to physical sheaths must be mentioned. We have seen that, in our model, the measured angular dispersion of the ion flux emerging from the sheath is due mainly to Coulomb "heating" near the plasma-sheath boundary, where the ion density is largest and the stream velocity is smallest. However, our assumption of an abruptly vanishing electron density that delimits this region from the plasma bulk is physically implausible; the introduction of a more realistic electron distribution would somewhat reduce (by virtue of its screening action) the transverse ion temperature that is realized.

Furthermore, depending on the ion-neutral and ion-ion "collisionality" in the plasma bulk, the assumption of a perfectly "cold" ion flux entering the sheath is also suspect. Any initial temperature of this flux would increase the angular dispersion $\theta_{\rm rms}$ measured at the cathode commensurately.

Since quantitative descriptions of the "presheath" region that separates the sheath from the plasma bulk are still in a rudimentary state (see, for example, [20]) we have chosen to omit these factors in our model. This also serves to simplify the analysis of the simulation results and to elucidate the essential physical behavior of an unscreened ion flux.

However, we have already seen in Sec. VI that simple diffusion theory explains the scaling of the angular dispersion $\theta_{\rm rms}$ reasonably well. Phenomenological descriptions of the effects of a finite initial ion temperature and a smoothly decreasing electron density can easily be incorporated in this theory. Thus, integrating Eq. (42) from an initial temperature $\Theta_0 = kT_0/mu_0^2 \neq 0$ at the plasma-sheath boundary and taking the electrons into account, we write

$$\theta_{\rm rms} \approx \frac{1}{\eta(\delta)} \left[(2\Theta_0)^{3/2} + \frac{4}{3\sqrt{\pi}} \frac{\Omega}{N_D} \int_0^{\delta} \nu^2(\zeta) \ln\Lambda(\zeta) d\zeta \right]^{1/3}, \quad (46)$$

where the function $\ln\Lambda(\zeta)$ is supposed to describe the diminution of Debye screening with penetration into the sheath [its variation is relatively weak; the upper cutoff $\beta_{\rm max}$ increases from unity to $\sim 10\delta$ (see Sec. V above)]. Under typical discharge conditions we expect $\Theta_0 \gtrsim 1$, and the initial-temperature term will dominate the sheath term in (46); for a physical sheath, set $\Omega = 1$.

Qualitatively, the above results may be understood by regarding the ion transport problem as an adiabatic expansion, in which the "self-collision" time [see Eq. (5-26) in [1]) is small compared to the "expansion" (sheath-traversal) time for typical sheath parameters. Under such circumstances, one expects the transverse ion temperature $T_\perp$ to be roughly constant, while the longitudinal temperature $T_\parallel$ varies as n^2 [1]. This agrees qualitatively with the behavior seen in Fig. 11.

VIII. CONCLUSION

We have shown empirically that, notwithstanding the absence of (electron) Debye screening, discrete Coulomb interactions are incapable of inducing a significant angular dispersion in the flux of ions traversing a unipolar plasma sheath under typical discharge conditions. This result may be attributable to the fact that even "non-neutral" plasmas exhibit a form of Debye screening [23]. Ordinarily, the observed angular dispersion of the ion flux will be determined by ion-neutral collisions and/or the initial ion temperature at the plasma-sheath boundary.

APPENDIX A: THE INTEGRATION SCHEME

To integrate the equations of motion (33), we have employed a fourth-order predictor-corrector scheme with individually adjusted time steps, based on methods developed for the gravitational N-body problem [26]. In the present context, great accuracy in the integration of ion trajectories is desired, since we wish to monitor deviations from linearity that are typically very small.

Let $\boldsymbol{\alpha} = d^2\boldsymbol{\xi}/d\tau^2$ be the dimensionless acceleration of a specific particle. As seen from Eq. (33), $\boldsymbol{\alpha}$ is obtained by summing contributions from the $N-1$ other particles and the smooth field $\mathcal{E}_S$. If $\boldsymbol{\alpha}_0$ and $\boldsymbol{\alpha}_{-1}, \boldsymbol{\alpha}_{-2}, \boldsymbol{\alpha}_{-3}$ are computed accelerations of the given particle at its current time τ_0 and at earlier times $\tau_{-1}, \tau_{-2}, \tau_{-3}$ (in order), then the cubic polynomial

$$\begin{aligned}\boldsymbol{\alpha}(\tau) = \boldsymbol{\alpha}_0 &+ \boldsymbol{\alpha}[\tau_{-1}, \tau_0](\tau - \tau_0) \\ &+ \boldsymbol{\alpha}[\tau_{-2}, \tau_{-1}, \tau_0](\tau - \tau_0)(\tau - \tau_{-1}) \\ &+ \boldsymbol{\alpha}[\tau_{-3}, \tau_{-2}, \tau_{-1}, \tau_0](\tau - \tau_0)(\tau - \tau_{-1})(\tau - \tau_{-2})\end{aligned} \quad (A1)$$

that interpolates these values is used to step the particle to the new time τ_1.

Integrating (A1) from τ_0 to τ_1 once and twice gives predicted increments for the particle velocity and location; "correction" terms may then be added after the particle acceleration α_1 at time τ_1 has been computed by means of an explicit summation in Eq. (33). Since the particles proceed on an "asynchronous" time front, a lower-order extrapolation of their coordinates to the common time τ_1 is required in order to compute α_1.

In Eq. (A1), the quantities $\alpha[\tau_{-k},\ldots,\tau_0]$ represent first, second, and third backward-divided-differences of the acceleration, defined recursively as

$$\alpha[\tau_{-1},\tau_0]=\frac{\alpha_0-\alpha_{-1}}{\tau_0-\tau_{-1}} ,$$

$$\alpha[\tau_{-2},\tau_{-1},\tau_0]=\frac{\alpha[\tau_{-1},\tau_0]-\alpha[\tau_{-2},\tau_{-1}]}{\tau_0-\tau_{-2}} , \tag{A2}$$

$$\alpha[\tau_{-3},\tau_{-2},\tau_{-1},\tau_0]=\frac{\alpha[\tau_{-2},\tau_{-1},\tau_0]-\alpha[\tau_{-3},\tau_{-2},\tau_{-1}]}{\tau_0-\tau_{-3}} .$$

The above forms facilitate an efficient updating of the coefficients in (A1) once the current time step for the given particle has been executed.

To start up the integration scheme, we need initial values for the backward-divided-differences (A2). These may be obtained by a symbolic differentiation of Eq. (33) three times, expressing the derivatives $\alpha',\alpha'',\alpha'''$ of the acceleration $\alpha=\xi''$ explicitly in terms of the initial positions ξ and velocities $\eta=\xi'$ of the particles. The N-body term gives rise to rather cumbersome expressions, which are enumerated in [26]. For the smooth-field term in (33), differentiating $\alpha=\mathcal{E}_S(\xi)$ three times gives

$$\alpha'=(\eta\cdot\nabla)\mathcal{E}_S ,$$

$$\alpha''=(\alpha\cdot\nabla)\mathcal{E}_S+(\eta\cdot\nabla)^2\mathcal{E}_S , \tag{A3}$$

$$\alpha'''=(\alpha'\cdot\nabla)\mathcal{E}_S+3(\eta\cdot\nabla)(\alpha\cdot\nabla)\mathcal{E}_S+(\eta\cdot\nabla)^3\mathcal{E}_S ,$$

where ∇ is the spatial gradient operator $\partial/\partial\xi$. In order to evaluate the above quantities at the location ξ_k of each particle, we need all derivatives—in Cartesian coordinates—of the potentials (17) and (31) to fourth order; their computation is tedious but straightforward.

Backward-divided-differences are then obtained from the derivatives $\alpha_0',\alpha_0'',\alpha_0'''$ at time τ_0 by choosing $\tau_0-\tau_{-k}=k\Delta\tau$ and equating the coefficients of each power of $\tau-\tau_0$ in (A1) with those of the truncated Taylor series

$$\alpha(\tau)=\alpha_0+\alpha_0'(\tau-\tau_0)+\frac{\alpha_0''}{2}(\tau-\tau_0)^2+\frac{\alpha_0'''}{6}(\tau-\tau_0)^3 . \tag{A4}$$

An adaptive time-step selection procedure was used, allowing a uniformly accurate integration of particle trajectories under fluctuating force fields or close encounters. Typically, the nominal distance traveled by any ion in a single time step does not exceed 5% of the sheath thickness, and the nominal fractional change in its speed or acceleration is also no more than 5%.

As a check on the integration accuracy, we monitor the "adjusted" system energy, defined at each instant in terms of the particle locations ξ_k and velocities η_k by

$$U=\sum_{k=1}^{N}\tfrac{1}{2}|\eta_k|^2+\sum_{j=1}^{N-1}\sum_{k=j+1}^{N}\frac{\Gamma_N}{(|\xi_j-\xi_k|^2+2\sigma^2)^{1/2}}+\sum_{k=1}^{N}\Phi_S(\xi_k)+\Delta U . \tag{A5}$$

Here the quantity ΔU represents the energy (kinetic plus potential) of each particle absorbed at the cathode minus that of each particle injected at the plasma-sheath boundary during the course of the simulation. $\Phi_S(\xi)$ is the potential associated with the smooth field $\mathcal{E}_S(\xi)$.

Since the total energy U given by (A5) is typically just a small difference between large kinetic and potential terms of opposite sign, we measure the cumulative error

$$\delta U=U_{\text{final}}-U_{\text{initial}}$$

relative to the sum of the absolute values of the kinetic and potential energies. Fractional errors were confined to the range 10^{-4}–10^{-6} for the simulations described herein. The longest runs took several CPU days on an IBM RS/6000 540 computer.

Finally, we note that efficient N-body schemes have been formulated [27] based on updating the force contributions of "near neighbors" and distant particles at different frequencies. This can give a significant speedup, the computing cost being roughly proportional to $N^{1.4}$ instead of N^2 for large N. Since our main interest here is to assess the contributions of interactions on different length scales to the (small) overall deflections of particles, however, we opt against the nearest-neighbor method because of concerns that it may incur a subtle systematic bias between short- and long-range interactions.

APPENDIX B: POTENTIAL OF A UNIFORM DISK

In cylindrical coordinates (r,ϕ,z) the potential due to a uniformly charged disk of radius a, centered on the origin in the plane $z=0$, is proportional to

$$S(r,z)=\int_0^a\int_{-\pi}^{+\pi}\frac{r'\,d\varphi\,dr'}{(r'^2-2rr'\cos\varphi+r^2+z^2)^{1/2}} . \tag{B1}$$

Standard texts on potential theory [28,29] mention this problem only in the trivial case $r=0$, for which we have

$$S(0,z)=2\pi[(z^2+a^2)^{1/2}-|z|] . \tag{B2}$$

In order to determine the potential (28) at arbitrary points in the simulation control volume, we need procedures to evaluate (B1) at nonzero values of r.

Treating the integral over φ first, we use [30, Eqs. 291.00 and 110.06]

$$\int_{-\pi}^{+\pi}\frac{d\theta}{\sqrt{a-b\cos\theta}}=\frac{4K(k)}{\sqrt{a+b}},\quad k=\left[\frac{2b}{a+b}\right]^{1/2} , \tag{B3}$$

where $K(k)$ denotes the complete elliptic integral of the first kind,

$$K(k)=\int_0^{\pi/2}\frac{d\phi}{(1-k^2\sin^2\phi)^{1/2}} . \tag{B4}$$

For $0\le k<1$, this may be readily evaluated using the convergent series

$$K(k)=\frac{\pi}{2}\left[1+\left[\frac{1}{2}\right]^2k^2+\left[\frac{1\times3}{2\times4}\right]^2k^4+\left[\frac{1\times3\times5}{2\times4\times6}\right]^2k^6+\cdots\right] . \tag{B5}$$

Thus we may express the potential (B1) in the form

$$S(r,z)=4\int_0^a\frac{K(k)r'dr'}{[(r'+r)^2+z^2]^{1/2}} ,$$

$$\text{where } k=\left[\frac{4rr'}{(r'+r)^2+z^2}\right]^{1/2} . \tag{B6}$$

This integral does not appear to admit any further straightforward reduction explicitly in terms of elliptic functions. Except for the singularity of K at $r'=r$ when $z=0$, however, it is not difficult to treat numerically.

We can also approach (B1) by integrating over r' first. Thus, making use of the standard result [31],

$$\int\frac{x\,dx}{(x^2+2px+q)^{1/2}}=(x^2+2px+q)^{1/2}-p\ln[(x^2+2px+q)^{1/2}+x+p] , \tag{B7}$$

the integral over r' yields the following four terms

$$(a^2-2ar\cos\varphi+r^2+z^2)^{1/2}-(r^2+z^2)^{1/2}+r\cos\varphi\ln[(a^2-2ar\cos\varphi+r^2+z^2)^{1/2}+a-r\cos\varphi]-r\cos\varphi\ln[(r^2+z^2)^{1/2}-r\cos\varphi] , \tag{B8}$$

which must then be integrated separately with respect to φ. In each case, it suffices to take twice the value of the integral over $\varphi\in[0,\pi]$ since these terms are all even functions of φ.

To investigate the first term in (B8), we use [30, Eqs. 291.05, 315.02, and 110.07]:

$$\int_0^\pi\sqrt{a-b\cos\theta}\,d\theta=2\sqrt{a+b}\,E(k),\quad k=\left[\frac{2b}{a+b}\right]^{1/2} , \tag{B9}$$

where the complete elliptic integral of the second kind

$$E(k)=\int_0^{\pi/2}(1-k^2\sin^2\phi)^{1/2}d\phi \tag{B10}$$

has the power-series representation

$$E(k)=\frac{\pi}{2}\left[1-\left[\frac{1}{2}\right]^2k^2-\left[\frac{1\times3}{2\times4}\right]^2\frac{k^4}{3}-\left[\frac{1\times3\times5}{2\times4\times6}\right]^2\frac{k^6}{5}-\cdots\right] , \tag{B11}$$

convergent for $0\le k\le1$. Thus the first term of (B8) contributes

$$S_1(r,z)=4[(r+a)^2+z^2]^{1/2}E(k) ,$$

$$\text{where } k=\left[\frac{4ar}{(r+a)^2+z^2}\right]^{1/2} , \tag{B12}$$

to $S(r,z)$, while the contribution of the second term is evidently just

$$S_2(r,z)=-2\pi(r^2+z^2)^{1/2} . \tag{B13}$$

The final term in (B8) is amenable to integration by parts. Differentiating the logarithmic factor and integrating $r\cos\varphi$, we obtain

$$-\{r\sin\varphi\ln[(r^2+z^2)^{1/2}-r\cos\varphi]\}_0^\pi+\int_0^\pi\frac{r^2\sin^2\varphi\,d\varphi}{(r^2+z^2)^{1/2}-r\cos\varphi} \tag{B14}$$

for the integral of this term from 0 to π. The first expression above clearly vanishes, while the second may be transformed by the substitution

$$\xi=(r^2+z^2)^{1/2}-r\cos\varphi \tag{B15}$$

into the integral

$$\int_{(r^2+z^2)^{1/2}-r}^{(r^2+z^2)^{1/2}+r}\frac{[-\xi^2+2(r^2+z^2)^{1/2}\xi-z^2]^{1/2}}{\xi}d\xi . \tag{B16}$$

The latter may be evaluated by using the result [31]

$$\int\frac{(ax^2+2bx+c)^{1/2}}{x}dx=(ax^2+2bx+c)^{1/2}-\frac{b}{\sqrt{-a}}\sin^{-1}\left[\frac{ax+b}{(b^2-ac)^{1/2}}\right]-\sqrt{-c}\,\sin^{-1}\left[\frac{bx+c}{|x|(b^2-ac)^{1/2}}\right] , \tag{B17}$$

where $a<0$ and $c<0$. Taking the difference between (B17) evaluated at $(r^2+z^2)^{1/2}+r$ and $(r^2+z^2)^{1/2}-r$, we find that the contribution of the last term in (B8) to the potential is

$$S_4(r,z)=2\pi[(r^2+z^2)^{1/2}-|z|] . \tag{B18}$$

Note that the first part of (B18) cancels the contribution (B13).

The integral of the third term in (B8) does not appear to have a simple resolution into elementary or elliptic functions. If we try to use integration by parts again to remove the logarithm, we obtain the form

$$-\int_0^\pi\frac{r^2-ar\cos\varphi+z^2}{(a^2-2ar\cos\varphi+r^2+z^2)^{1/2}}\frac{r^2\sin^2\varphi\,d\varphi}{r^2\sin^2\varphi+z^2} \tag{B19}$$

after some manipulation. This has no further obvious reduction; we therefore resort to a numerical quadrature for the third term in (B8).

[1] L. Spitzer, Jr., *Physics of Fully Ionized Gases* (Wiley, New York, 1962), Chap. 5.
[2] S. Chandrasekhar, *Principles of Stellar Dynamics* (Dover, New York, 1960), Chap. 2.
[3] H. E. Kandrup, Phys. Rep. **63**, 1 (1980).
[4] R. T. Farouki and E. E. Salpeter, Astrophys. J. **253**, 512 (1982).
[5] *VLSI Technology,* edited by S. M. Sze (McGraw-Hill, New York, 1988), Chap. 8.
[6] M. J. Kushner, J. Appl. Phys. **58**, 4024 (1985).
[7] B. E. Thompson, H. H. Sawin, and D. A. Fisher, J. Appl. Phys. **63**, 2241 (1988).
[8] J. I. Ulacia F. and J. P. McVittie, J. Appl. Phys. **65**, 1484 (1989).
[9] R. T. Farouki, S. Hamaguchi, and M. Dalvie, Phys. Rev. A **44**, 2664 (1991).
[10] M. S. Barnes, J. C. Forster, and J. H. Keller, IEEE Trans. Plasma Sci. **PS-19**, 240 (1991).
[11] E. A. Mason and E. W. McDaniel, *Transport Properties of Ions in Gases* (Wiley, New York, 1988).
[12] C. K. Birdsall and A. B. Langdon, *Plasma Physics via Computer Simulation* (McGraw-Hill, New York, 1985).
[13] S. Chandrasekhar, Astrophys. J. **97**, 255 (1943).
[14] S. Chandrasekhar, Rev. Mod. Phys. **15**, 1 (1943).
[15] P. C. Clemmow and J. P. Dougherty, *Electrodynamics of Particles and Plasmas* (Addison-Wesley, Reading, MA, 1969), Chap. 12.
[16] R. S. Cohen, L. Spitzer, Jr., and P. McR. Routly, Phys. Rev. **80**, 230 (1950).
[17] S. Gasiorowicz, M. Neuman, and R. J. Riddell, Jr., Phys. Rev. **101**, 922 (1956).
[18] M. N. Rosenbluth, W. M. MacDonald, and D. L. Judd, Phys. Rev. **107**, 1 (1957).
[19] D. Bohm, in *The Characteristics of Electrical Discharges in Magnetic Fields,* edited by A. Guthrie and R. K. Wakerling (McGraw-Hill, New York, 1949), Chap. 3.
[20] K.-U. Riemann, J. Phys. D **24**, 493 (1991).
[21] R. T. Farouki, M. Dalvie, and L. F. Pavarino, J. Appl. Phys. **68**, 6106 (1990).
[22] C. de Boor, *A Practical Guide to Splines* (Springer, New York, 1978).
[23] R. C. Davidson, J. Plasma Phys. **6**, 229 (1971).
[24] C. D. Child, Phys. Rev. **32**, 492 (1911).
[25] I. Langmuir, Phys. Rev. (Ser. II) **2**, 450 (1913).
[26] S. J. Aarseth, in *The Gravitational N-Body Problem,* edited by M. Lecar (Reidel, Dordrecht, 1972), p. 373.
[27] A. Ahmad and L. Cohen, J. Comput. Phys. **12**, 389 (1973).
[28] O. D. Kellogg, *Foundations of Potential Theory* (Ungar, New York, 1970).
[29] W. J. Sternberg and T. L. Smith, *The Theory of Potential and Spherical Harmonics,* 2nd ed. (University of Toronto Press, Toronto, 1952).
[30] P. F. Byrd and M. D. Friedman, *Handbook of Elliptic Integrals for Engineers and Scientists,* 2nd ed. (Springer, New York, 1971).
[31] I. S. Gradshteyn and I. M. Ryzhik, *Tables of Integrals, Series, and Products* (Academic, New York, 1980).